

This manuscript has been submitted for publication in Water Resources Research. Please note that it has not been peer-reviewed and has not yet been accepted for publication. Subsequent versions of this manuscript may have different content. If accepted, the final version of this manuscript will be available via the 'Peer reviewed Publication DOI' link on the right-hand side of this webpage. Please feel free to contact any of the authors; we welcome feedback.

1 **Intercomparison of deep learning architectures for the**
2 **prediction of precipitation fields**

3 **Noelia Otero and Pascal Horton**

4 ¹Institute of Geography and Oeschger Centre for Climate Change Research, University of Bern, Bern,
5 Switzerland

Abstract

In recent years, the use of deep learning methods has rapidly increased in many research fields. Similarly, they have become a powerful tool within the climate scientific community. Deep learning methods have been successfully applied for different tasks, such as identification of atmospheric patterns, weather extreme classification, or weather forecasting. However, due to the inherent complexity of the atmospheric processes, the ability of deep learning models to simulate natural processes, such as precipitation, is still challenging. Therefore, a thorough evaluation of their performance and robustness in predicting precipitation fields is still needed, especially for extreme precipitation events, which can be devastating in terms of infrastructure damage, economic losses, and even loss of life. In this study, we present a comprehensive evaluation of a set of deep learning architectures to realistically simulate precipitation, including heavy precipitation events (>95th percentile) and extreme events (>99th percentile) over the European domain. Moreover, we examine the optimal number of inputs based on the importance of the predictors derived from a layer-wise relevance propagation procedure. Among the architectures analyzed here, the U-Net network was found to be superior and outperformed the other networks to simulate precipitation events. Moreover, we found that a simplified version of the original U-Net with a single encoder-decoder level achieves similar skill scores as deeper versions for predicting precipitation extremes, significantly reducing overall complexity and computing resources.

Plain Language Summary

With the increasing success of machine learning methods in Earth Sciences, deep learning is becoming a promising tool for building data-driven models for meteorological applications. Yet, predicting extreme events, such as heavy rainfall, is still challenging. We present an intercomparison of deep learning models to assess the capability of different architectures to predict precipitation events.

1 Introduction

Predicting precipitation is challenging for numerical weather prediction (NWP) models. Precipitation involves complex microphysical processes that cannot be explicitly resolved in most models due to inadequate grid resolution and high computational requirements. Such processes are inferred from parametrization schemes, which are generally sources of parametric uncertainty (Bauer et al., 2015). NPW models solve numerically coupled partial differential equations subject to dynamic and thermodynamic laws that describe the atmospheric state (Schultz et al., 2021). Therefore, NPW models are computationally expensive.

A major concern relates to extreme precipitation events that are expected to change in intensity and frequency under a changing climate, leading to higher socio-economic impacts (Trenberth et al., 2003; Donat et al., 2016). The skill of climate models, or more specifically general circulation models (GCM), to predict extreme events is rather limited due to their lack of ability to represent mesoscale processes that require higher spatio-temporal resolutions (Gao & A., 2019). Regional climate models (RCM) can better represent topography and small-scale microphysical processes thanks to a higher spatial resolution (2–25 km) but are computationally expensive (Adewoyin et al., 2021). Alternatively, statistical downscaling techniques can establish relationships between large-scale variables (predictors) and the variable of interest (predictand) (Maraun et al., 2017).

With the rapid development of machine learning (ML) techniques, sophisticated deep learning (DL) models, and the availability of large data sets, there is an increasing interest in the weather and climate research community to tackle climate-related problems using ML. ML models can extract high-level feature representations from observed patterns and relate them to general meteorological situations. Moreover, ML models are computationally much cheaper than physically-based modeling of the physical processes responsible for precipita-

55 tion. Recent studies have proposed different ML methods and DL architectures to predict
56 precipitation at several time scales, including nowcasting, sub-seasonal, and seasonal fore-
57 cast (Vandal et al., 2019; Hwang et al., 2019; Civitarese et al., 2021). These ML applications
58 have shown promising results for predicting precipitation (Adewoyin et al., 2021).

59 Data-driven approaches have become very popular in many fields of natural sciences
60 due to their ability to learn and efficiently represent underlying physical processes (Rasp et
61 al., 2020). Several studies have shown the great potential of convolutional neuronal network
62 (CNN) architectures to reproduce synoptic patterns (Chattopadhyay et al., 2020), weather
63 extreme events (Liu et al., 2016), and provide weather forecasting (Weyn et al., 2019; Scher,
64 2018). In particular, precipitation forecasting has been the subject of DL studies that have
65 proposed advanced network architectures that can outperform conventional forecast models
66 (Rasp et al., 2020).

67 Previous works have used DL to predict extreme precipitation for spatially aggregated
68 time series (Davenport & Diffenbaugh, 2021; Huang, 2022) or to predict high-resolution
69 precipitation locally (i.e., statistical downscaling) (Adewoyin et al., 2021; Pan et al., 2019).
70 However, the extreme values in the predicted precipitation fields over a larger domain have
71 not yet been investigated enough nor improved. Therefore, this work aims to fill this gap by
72 assessing the performance of existing DL models to predict spatial precipitation extremes.
73 Building upon recent works, we present an intercomparison of DL architectures and assess
74 their ability to predict extreme precipitation events over Europe. While our primary focus
75 is to test the model performance to capture precipitation extremes, we also examine the DL
76 performance for precipitation estimates. Contrasting with most of the existing literature
77 where the domain of interest focused on precipitation over the U.S. (e.g., Davenport & Dif-
78 fenbaugh, 2021; Pan et al., 2019), here we present a model comparison over the European
79 domain. The skills of the models are compared for the prediction of the spatial precipitation
80 amount as well as for the spatial probability of exceedance of the 95th (i.e., heavy precipita-
81 tion) and 99th (i.e., extreme precipitation) percentiles. In a second step, we conduct several
82 experiments to assess the effect of the model depth. Furthermore, we apply a layer-wise
83 relevance propagation (LWR) method to interpret the role of the different input features for
84 heavy precipitation events and evaluate the optimal number of input data.

85 The rest of the paper is organized as follows: Section 2 discusses previous related work.
86 The data and methods are introduced in Section 3. Section 4 shows the results and the
87 main conclusions are summarized in Section 5.

88 2 Related works

89 Recently, many studies have proposed using sophisticated ML methods to improve
90 precipitation estimates in various contexts, such as precipitation nowcasting (Ayzel et al.,
91 2019) and post-processing of NWP precipitation output (Hess & Boers, 2022). This section
92 reviews the most relevant studies closely related to our objectives and methodology.

93 Davenport and Diffenbaugh (2021) analyzed extreme precipitation days (above 95th
94 percentile) over the U.S. Midwest and their links to large-scale atmospheric circulation
95 patterns using a CNN with daily sea level pressure and geopotential height anomalies as
96 input fields (Table 1). The model architecture consisted of two convolutional layers, each
97 followed by a max-pooling layer, a dense 16-neuron layer, and a final classification layer
98 of extreme and non-extreme precipitation days. The CNN showed high accuracy (91%)
99 for the identification of extreme precipitation days, although some extreme events were
100 not captured. The authors suggested that additional variables representing smaller-scale
101 processes might improve the model performance. Moreover, due to the differences in the
102 seasonal distribution of precipitation during extreme events, they pointed out the relevance
103 of incorporating temporal information.

104 Building upon the work of Davenport and Diffenbaugh (2021), Huang (2022) proposed a
105 self-attention augmented convolution mechanism for short-term extreme precipitation fore-
106 casting over the U.S. Midwest. The network consisted of two attention-augmented con-
107 volutional layers, a max-pooling, and a dropout layer. The proposed model outperformed
108 classical convolutional models by 12%. However, a limitation to capturing some extreme
109 events was acknowledged, likely due to localized processes for which additional information
110 (e.g., variables) might be required.

111 Focusing on precipitation downscaling to point locations, Pan et al. (2019) proposed
112 a CNN model as an alternative to parameterization schemes for numerical precipitation
113 estimation. They built a CNN model based on convolutional and pooling layers using the
114 geopotential height at several pressure levels and the total column water as inputs (at a
115 3-hourly time step; see Table 1). The extracted features were flattened and processed by
116 two final dense layers. The authors tested the CNN in different locations across the U.S.
117 and showed that the CNN outperformed the reanalysis precipitation products and classical
118 statistical methods. However, the model underestimated large precipitation values.

119 Similarly, Shi (2020) evaluated the performance of ML methods, including CNNs, for
120 statistical downscaling of extreme precipitation in three Asian regions. They compared two
121 DL architectures, RaNet with three convolutional layers and five fully connected layers,
122 and RxNet, a more complex model with 58 layers, including residual connections similar
123 to the original Xception model (Chollet, 2017). The results showed that deep CNN with
124 an intermediate-level complexity structure (e.g., RaNet) generally performed better than
125 a more complex architecture (e.g., RxNet). Moreover, while the CNNs well captured the
126 precipitation extremes in the subtropical regions, they performed poorly in the tropical
127 regions, illustrating the challenge of representing extreme precipitation in certain regions.

128 Adewoyin et al. (2021) developed TRU-NET (Temporal Recurrent U-Net), a DL model
129 based on a U-Net (Sect. 3.2.1) architecture and featuring a novel 2D cross attention mech-
130 anism to account for the spatio-temporal nature of weather processes. It relies on Convolu-
131 tional Long Short-Term Memory (ConvLSTM) cells, more specifically Convolutional Gated
132 Recurrent Units (ConvGRU). Their objective is to improve the prediction of high-resolution
133 precipitation for climate models, which provide low-resolution outputs. They used 6 model
134 fields as input, including mean sea level pressure, geopotential height, specific humidity,
135 water vapor, and wind components (Table 1), at a 65 km spatial resolution and 6-hourly
136 time step to predict precipitation over the UK at an 8.5 km resolution. The outputs are the
137 rainfall probabilities and the rainfall values. The TRU-NET architecture captures the vari-
138 ability at different spatio-temporal scales through its 3-layers encoder: from six-hourly/8.5
139 km, to daily/34 km, and to weekly/136 km. They propose a Fused Temporal Cross Atten-
140 tion (FTCA) as a better aggregation strategy than averaging the six-hourly data to a daily
141 time step. They show that TRU-NET outperforms other models, including U-Net, and
142 conclude that this is due to its ability to use the temporal information present in weather
143 data. However, they notice that TRU-NET under-predicts high precipitation events (> 20
144 mm/d).

145 Recently, Hess and Boers (2022) showed that a U-Net-based network, using NWP
146 ensemble simulations as input features, captures well heavy rainfall events. They applied
147 DL as a post-processing step to correct biases in the NWP-predicted rainfall. They proposed
148 a frequency-based weighting of the loss function that combines a continuously weighted mean
149 square error (MSE) with a multi-scale structural similarity measure, which improved the
150 training for high values when using both metrics separately.

3 Data and Methods

3.1 Data

The input variables and the precipitation fields were retrieved from the ERA5 (Hersbach et al., 2020) reanalysis. Reanalyses are produced using a single version of a data assimilation system coupled with a forecast model constrained to follow observations over a long period. They provide multivariate outputs that are physically consistent, also for variables that are not directly observed (Gelaro et al., 2017). ERA5 is the state-of-the-art reanalysis at the time of writing and was shown to outperform other reanalyses for predicting precipitation using a simpler statistical downscaling method (Horton, 2021). ERA5 provides data with high temporal (hourly) and spatial (0.25°) resolutions.

The weather variables used as input to the DL model should be robust, i.e., not depend too much on the climate model or the NWP model, for the DL model to be transferable to other contexts (Adewoyin et al., 2021). We thus selected frequently-used variables: geopotential height (Z), air temperature (T), relative humidity (RH), total column water (TCW), and both wind components (U, V). All variables were selected at six pressure levels, i.e., 300, 500, 700, 850, 925, and 1000 hPa, except the total column water, which has a single vertical dimension. To reduce the computational costs of training all the networks (see Section 3.2), the spatial resolution of ERA5 data was degraded to 1° . Additionally, the variables were temporally aggregated at a daily time step. The domain on which these variables are used is: latitude = [30, 75] and longitude = [-25, 30].

The precipitation data were also extracted from ERA5 over the same domain and spatial resolution (1°) and aggregated to a daily time step. Our study period is from 1979 to 2021. In this work, heavy precipitation events are identified based on the 95th percentile of the total distribution (1979-2021) for each grid cell (i.e., pixel-wise definition). Similarly, extreme precipitation events are defined as those days exceeding the 99th percentile (Figure S1).

3.2 Methods

3.2.1 Deep Convolutional Neural Networks: selected architectures

CNNs have proven successful in different applications in climate science, including extreme weather forecasting (Racah et al., 2016; Liu et al., 2016), clustered weather patterns prediction (Chattopadhyay et al., 2020), precipitation nowcasting (Shi et al., 2015, 2017), or extreme precipitation (Davenport & Duffenbaugh, 2021; Shi, 2020). They are a type of neural network designed to process high-dimensional data, such as images or geospatial data (LeCun & Bengio, 1995). They have become tremendously popular due to their ability to automatically learn spatial hierarchies of features, from low to high-level patterns (Goodfellow et al., 2016). The principle of CNN relies on a mathematical operation called *convolution*, a specialized linear operation used for feature extraction (Goodfellow et al., 2016). CNNs usually consist of three types of layers: i) convolutional layers that perform the convolution operation, ii) pooling layers that reduce the dimensionality of the inputs, and iii) fully connected layers. The first two types of layers extract and condense the feature information used by dense layers. A typical CNN architecture is often composed of successive convolutional and pooling layers.

Building on CNNs, the popular U-Net, which was originally introduced by Ronneberger et al. (2015) for biomedical image segmentation, has shown good performance in climate applications, such as post-processing weather forecasts (Grönquist et al., 2021; Hess & Boers, 2022), downscaling (e.g., Adewoyin et al., 2021) and precipitation nowcasting (e.g., Trebing et al., 2021). Larraondo et al. (2019) tested several encoder-decoder configurations and found the best results with U-Net-based architectures to forecast total precipitation using geopotential height as input. In Weyn et al. (2020), the authors used a U-Net architecture

200 and mapped the input grid values to a cubed-sphere achieving a good performance to fore-
 201 cast complex surface temperature patterns from a few input atmospheric state variables.
 202 The U-Net architecture consists of two parts: a contracting path to capture the context
 203 (encoder) and a symmetric expanding path that enables precise localization (decoder). The
 204 encoder part is composed of stacked convolutions and pooling operations to extract the
 205 features, while the decoder part combines these features (through skip connections) with
 206 the upscaled output to reconstruct the spatial information. The encoder-decoder network
 207 enables propagating high-resolution features from the contracting path that are combined
 208 with the upscaled output (Ronneberger et al., 2015).

209 Among the DL models presented in the literature for predicting precipitation, we have
 210 selected a number of representative studies closely related to our objectives. Given that our
 211 approach and model domain differ from the selected original studies, we have adapted the
 212 original architectures to our purpose in each case. Table 1 summarizes the inputs originally
 213 used in the selected studies. Below, we briefly describe the models considered in our study:

- 214 • **Dav-orig**: The original CNN model presented in Davenport and Diffenbaugh (2021)
 215 includes two convolutional layers with 16 3x3 filters, followed by two 2x2 max-pooling
 216 with a stride of 2. In the original configuration, a dense 16-neuron layer follows the
 217 convolution and max-pooling layers, followed by a final classification layer providing
 218 the probability of the outcomes. To predict a spatial precipitation field over the
 219 European domain, we added a decoder part made of a dense layer, two deconvolution
 220 layers, and a final convolution layer, symmetrically to the original model. The model
 221 has 48,697 trainable parameters.
- 222 • **Dav-64**: We tested a different architecture based on Dav-orig with a latent space of
 223 dimension 64 instead of 16. It has 175,081 trainable parameters.
- 224 • **Pan-orig**: The CNN model used in Pan et al. (2019) consisted of two convolutional
 225 and pooling layers followed by two consecutive dense layers. As in the previous model
 226 configurations, a symmetrical decoder part was added to keep the spatial dimensions.
 227 The model has 233,014 trainable parameters.
- 228 • **CNN-2l**: Following the architectures described above, we additionally tested a con-
 229 volutional encoder-decoder made of two layers, with a latent space of dimension 64.
 230 Further experiments with additional layers were conducted but were not successful.
 231 Therefore, the results presented only refer to the CNN-2l. The model has 740,297
 232 trainable parameters.
- 233 • **U-Net**: With the success shown by the U-Net in diverse applications, we explored
 234 the performance of the original U-Net model with the same structure as proposed by
 235 Ronneberger et al. (2015). It has 31,059,073 trainable parameters.
- 236 • **Shi-RaNet**: Following the original RaNet architecture proposed in Shi (2020), this
 237 model consists of three 3-dimensional CNN layers (using three-dimensional filters) and
 238 four fully connected layers, followed by a symmetric decoder part of upscaling layers
 239 that allow reconstructing the output into its original size. The model has 1,859,627
 240 trainable parameters.

Table 1. Meteorological variables used by the selected studies. The variables are: sea-level pressure (SLP), geopotential height (Z), air temperature (T), specific humidity (SH), relative humidity (RH), the zonal and meridional wind components (U/V), the total column water vapor (TCW) or precipitable water (PW). The column 'Nb' contains the number of variables used. The table values for Z, T, SH, RH, and U/V represent the pressure levels selected (hPa).

Study	Nb	SLP	Z	T	SH	RH	U/V	TCW/PW
Davenport and Diffenbaugh (2021)	2	1x	500	–	–	–	–	–
Huang (2022)	2	1x	500	–	–	–	–	–
Pan et al. (2019)	4	–	500, 850, 1000	–	–	–	–	1x
Shi (2020)	30	–	300, 500, 700, 850, 925, 1000	300, 500, 700, 850, 925, 1000	–	300, 500, 700, 850, 925, 1000	300, 500, 700, 850, 925, 1000	–

3.2.2 Models implementation

While our primary goal is to assess the model performance to reproduce precipitation extremes, we also tested the models to predict precipitation amounts. Therefore, the implemented models were assessed for different objectives: i) for the prediction of the precipitation amount, ii) for the occurrence of heavy precipitation (i.e., > 95th percentile), and iii) for the occurrence of extremes (> 99th percentile). The model configuration is the same in all cases, the only difference being the activation function of the last layer. A rectified linear unit (ReLU) that ensures non-negative output values is used for predicting the precipitation amount and a sigmoid is applied for predicting the probability of heavy/extreme events. It is important to note that all models were trained independently. The loss function used was the mean squared error (MSE) for the prediction of the precipitation amount and the weighted binary cross-entropy for the prediction of the occurrence of extremes (with weights computed to balance both classes). These scores were computed pixel-wise and aggregated over the domain. An early-stopping strategy has been used, with a maximum of 200 epochs. For all models, dropout and spatial dropout for the convolutional layers have been used.

A class was written in Python to generate the different model architectures with multiple options and handle common tasks, such as an eventual initial zero-padding when necessary, and output cropping. It also sets the final activation layer to ReLU for the prediction of precipitation values or sigmoid for the prediction of the probability of extremes. The models were implemented using Keras (Chollet et al., 2015) and designed according to the description in the related paper.

The input data is a tensor of shape 46x56x31; 31 represents the number of atmospheric fields (i.e., channels): six fields for Z, RH, T, U, V, and one for TCW; 46x56 represents the spatial dimensions (latitude x longitude) of the domain considered. All models use the same number of channels (i.e., 31), except the Shi-RaNet model, for which TCW was excluded as 3D variables are required. The training period ranges from 1979 to 2005 and validation from 2005 to 2015. The testing period covers from 2016 to 2021.

3.2.3 Feature importance: Layer-wise Relevance propagation

We used layer-wise relevance propagation (LRP), an explanation technique applicable to ML models (e.g. Montavon et al., 2018), to better understand the importance of the input variables for heavy precipitation events, i.e., which variables are more important for the network to make a prediction. Among the existing methods of DL interpretation, LRP is a backward propagation technique used for explaining complex network outputs. The LRP creates heatmaps, which in our case help identify the most relevant regions of the input for predicting a heavy precipitation event (Barnes et al., 2022). Similarly to recent studies that used LRP in geoscience applications (e.g. Davenport & Duffenbaugh, 2021; Toms et al., 2020), we apply the α - β rule with $\alpha = 1$ and $\beta = 0$ to identify locations for which higher activation values positively contribute to a likely output (i.e. predicted class). Thus, with this formulation, only positive contributions to the neural network output are tracked. It is therefore well suited to categorical output (i.e., extreme or not extreme). We additionally tested other methods, such as the gradient and the deep Taylor, but for simplicity and easier output interpretation, we only considered the alpha-beta rule, specifically the $\alpha_0\beta_1$.

The LRP produces a map with the same dimensions as the input, where the pixel values indicate the importance of the predicted class. A total of 31 maps (i.e., 31 input variables) are obtained for each day. Then, we computed composite maps (for each input feature separately) by calculating for every pixel the average value of the relevance of a specific input feature for all days with an extreme event at that same pixel, within the training period: $\bar{R} = \frac{1}{N_i} \sum R$. For comparison, we considered a larger area of influence for each pixel by calculating the averages of the maximum relevance within a small spatial domain for each feature when an event occurred:

$$\bar{R} = \frac{1}{N_i} \sum \max(R \mp z);$$

where z represents the number of the closest pixels to calculate the relevances at each grid cell. We performed additional sensitivity analyses for different values of z and decided to use $z = 3$ as a good compromise to account for local processes that might be relevant for pixel-wise precipitation events. It is important to note that the averages of the relevances were calculated for the *true* extremes.

As detailed below (see Section 4.3), after selecting our best model for predicting precipitation, we apply the LRP to examine the most important features for simulating heavy precipitation events. Based on the relevance values obtained for the training sample, we ranked the predictors by their average relevance. These values were obtained by averaging the composite maps produced for each input feature. Then, we conducted a number of experiments for differing subsets of predictors to examine the role of the number of features in the model performance.

4 Results

4.1 Networks performance

We noticed that the loss values greatly vary when comparing the architectures. Overall, the loss decreases relatively consistently for the different models. The U-Net shows the lowest values, and its optimization stops significantly earlier than other models (Figures S2, S3).

309 We trained the models separately predicting precipitation amounts (e.g. as a regression
 310 task) and precipitation events (e.g. as a classification task). In the first case, we assessed
 311 the prediction of the precipitation amount through the RMSE, and we further estimated
 312 the predicted threshold exceedances (95th and 99th percentile for each pixel) to compute
 313 the precision and recall scores (Table 2 for the 95th percentile and Table 3 for the 99th
 314 percentile). The U-Net outperformed the rest of the models for predicting precipitation
 315 amounts and provided the lower RSME and the highest precision and recall scores when
 316 assessing the threshold exceedances.

Table 2. Scores of the tested models when trained to **predict the precipitation amount**. Precision and recall are computed for the exceedance of the **95th percentile**. The best scores are highlighted in bold.

Model id	RMSE train	RMSE test	Precision train	Precision test	Recall train	Recall test
Dav-orig	3.19	3.33	0.55	0.51	0.21	0.20
Dav-64	2.74	2.93	0.65	0.62	0.37	0.34
Pan-orig	2.42	2.58	0.68	0.66	0.47	0.44
CNN-21	2.35	2.68	0.69	0.63	0.50	0.43
U-Net	1.43	1.73	0.81	0.78	0.69	0.64
Shi-RaNet	3.21	3.43	0.60	0.53	0.18	0.15

Table 3. Scores of the tested models when trained to **predict the precipitation amount**. Precision and recall are computed for the exceedance of the **99th percentile**. The best scores are highlighted in bold.

Model id	RMSE train	RMSE test	Precision train	Precision test	Recall train	Recall test
Dav-orig	3.21	3.35	0.31	0.13	0.02	0.02
Dav-64	2.73	2.91	0.58	0.46	0.16	0.12
Pan-orig	2.44	2.59	0.68	0.63	0.26	0.22
CNN-21	2.36	2.67	0.68	0.57	0.31	0.21
U-Net	1.46	1.73	0.84	0.79	0.52	0.43
Shi-RaNet	3.01	3.30	0.57	0.31	0.07	0.03

317 The forecast skills of heavy and extreme precipitation events were evaluated in terms
 318 of the AUC (ROC under curve area), the precision and recall scores based on a probability
 319 threshold of 0.5 Tables 4 and 5 show the score values obtained for classifying both heavy
 320 (>95th) and extreme (>99th) precipitation events.

321 Similarly to the regression case, the results show clearly that U-Net, which has signif-
 322 icantly more trainable parameters, is the best to predict precipitation extremes. However,
 323 a difference between both settings becomes obvious: when trained for the prediction of
 324 extremes, the model’s outputs result in a much higher recall than when trained for the pre-
 325 cipitation amount while presenting a lower precision. The models trained for the extremes
 326 predict them better than when trained for the whole precipitation distribution (i.e., Table
 327 3), but overestimate the number of extreme events (i.e., Table 5). It can be expected that
 328 balancing the weights differently in the weighted binary cross-entropy will result in other
 329 recall and precision scores.

Table 4. Scores of the tested models when trained to **predict precipitation extremes**. Precision and recall are computed for the exceedance of the **95th percentile**. The best scores are highlighted in bold.

Model id	AUC train	AUC test	Precision train	Precision test	Recall train	Recall test
Dav-orig	0.90	0.89	0.17	0.18	0.86	0.83
Dav-64	0.95	0.93	0.25	0.25	0.91	0.87
Pan-orig	0.96	0.95	0.26	0.26	0.95	0.92
CNN-2l	0.97	0.94	0.27	0.26	0.96	0.89
U-Net	0.99	0.98	0.38	0.38	0.99	0.95
Shi-RaNet	0.92	0.88	0.18	0.17	0.91	0.84

Table 5. Scores of the tested models when trained to **predict precipitation extremes**. Precision and recall are computed for the exceedance of the **99th percentile**. The best scores are highlighted in bold.

Model id	AUC train	AUC test	Precision train	Precision test	Recall train	Recall test
Dav-orig	0.94	0.92	0.05	0.05	0.93	0.89
Dav-64	0.98	0.96	0.10	0.09	0.96	0.88
Pan-orig	0.98	0.97	0.09	0.09	0.98	0.93
CNN-2l	0.97	0.94	0.07	0.07	0.97	0.89
U-Net	0.99	0.99	0.17	0.17	0.99	0.97
Shi-RaNet	0.93	0.89	0.05	0.05	0.92	0.80

330 We further analyze the ability of the models to represent the spatial distribution of
 331 precipitation events realistically. To do so, we examine the predictions of the different

332 models for the day with the highest amount of observed precipitation exceeding the 95th
333 percentile and the 99th percentile during the test period and over the considered domain.

334 Figures 1 and 2 show the results of the models trained for the prediction of the precip-
335 itation amount (two first columns) and the results of the models trained for the prediction
336 of the occurrence of extremes (last column). From Figure 1 it can be seen that, in general,
337 most of the models simulate fairly well heavy precipitation events. In particular, Dav-64,
338 Pan-orig and CNN-2l show consistent patterns when compared with the truth (i.e., ERA5).
339 The differences between the models become larger when comparing their performance in
340 capturing extreme precipitation events (Figure 2). In that case, it can be observed that
341 U-Net is superior and reproduces the closest pattern to the *truth*. In agreement with the
342 skill scores in Tables 2-5, the U-Net outperforms the rest of the models for both the amount
343 of precipitation and the threshold exceedances. Although U-Net simulates relatively well
344 the precipitation fields, as mentioned before, the model tends to predict a high number of
345 false positives, as shown by a lower precision skill (compared to the recall skill).

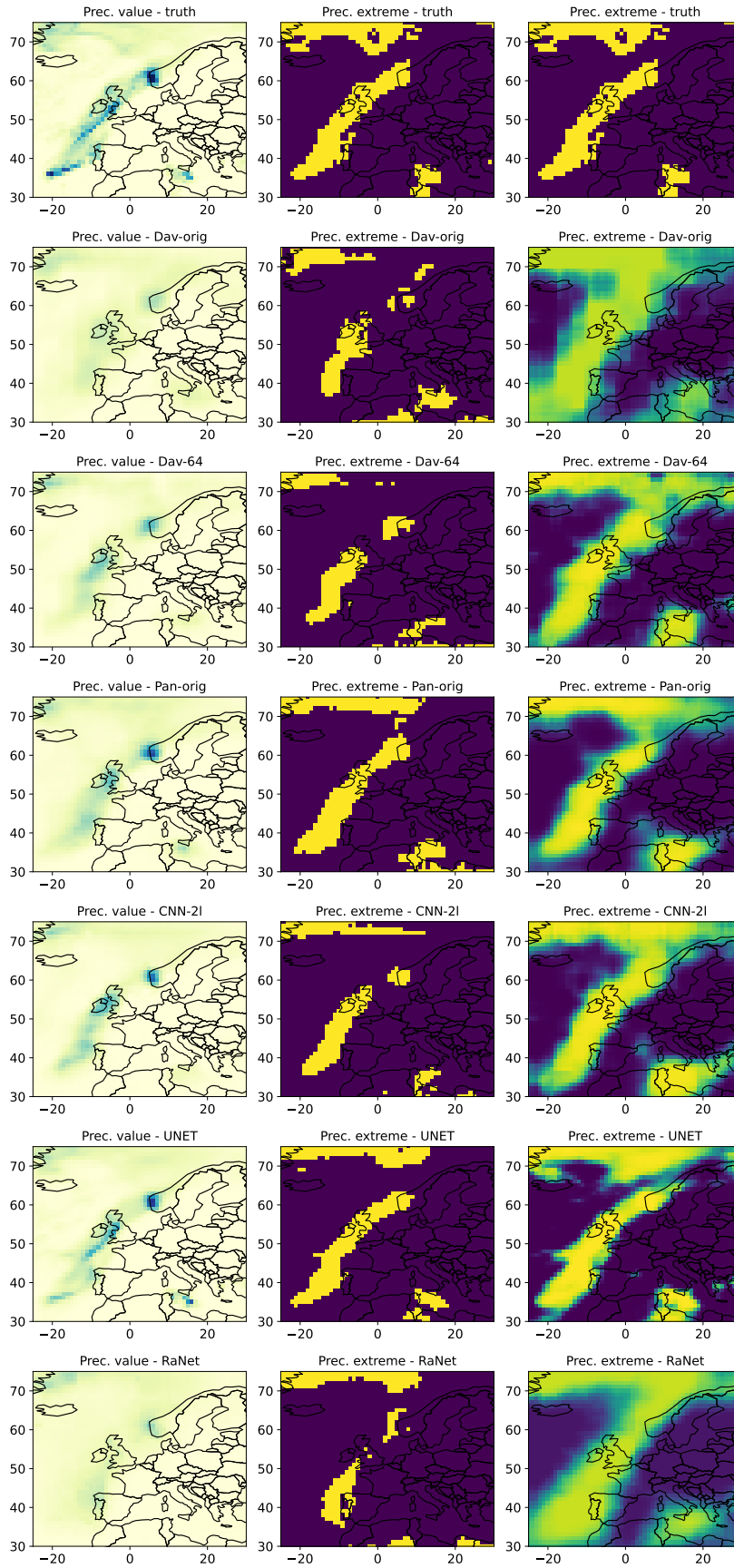


Figure 1. First row: true values of the precipitation amount and the corresponding threshold exceedance for the **95th percentile**. Next rows: the prediction of each model for the same date, in terms of precipitation amount (first column), the corresponding threshold exceedance (second column), and the probability of the occurrence of heavy precipitation (third column).

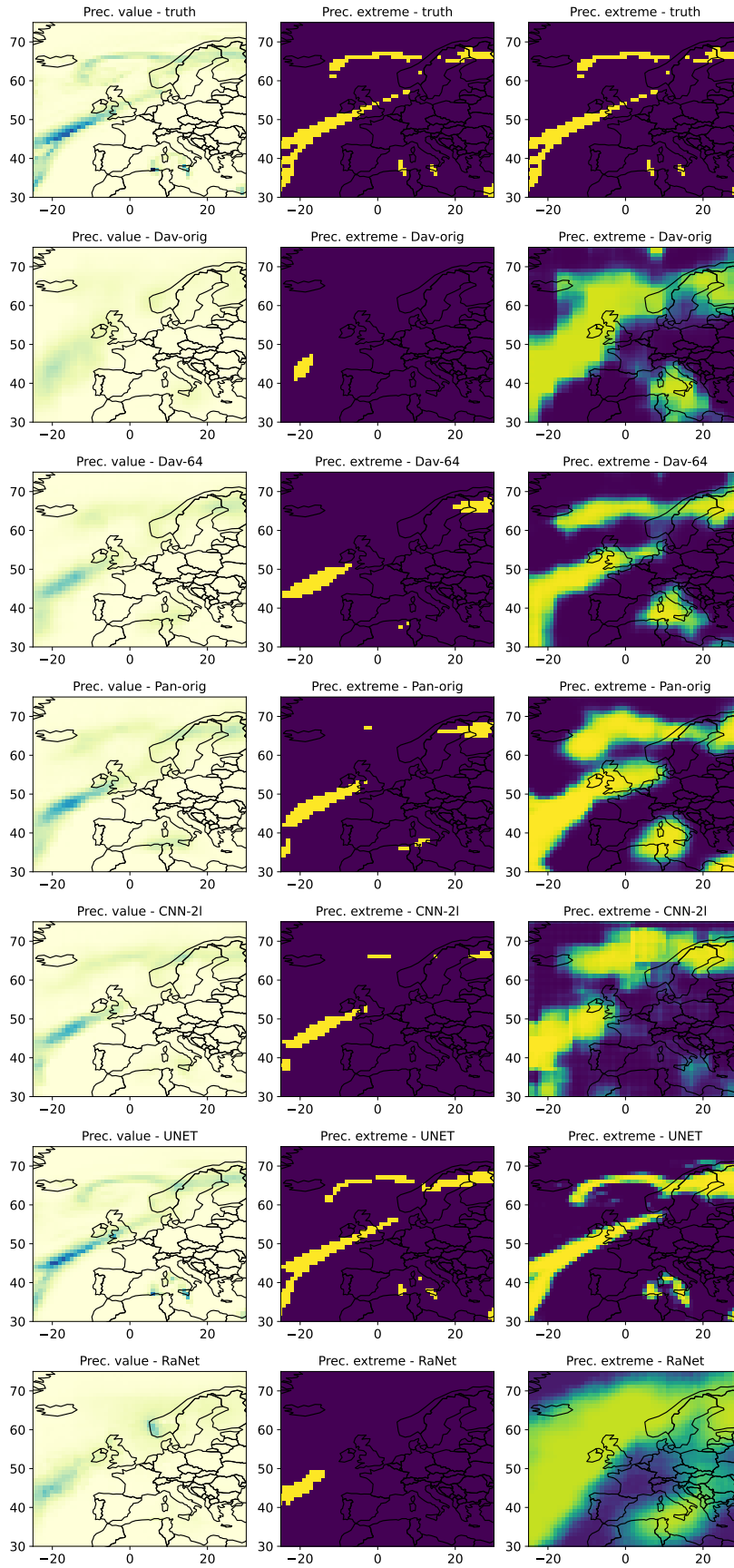


Figure 2. First row: true values of the precipitation amount and the corresponding threshold exceedance for the **99th percentile**. Next rows: the prediction of each model for the same date, in terms of precipitation amount (first column), the corresponding threshold exceedance (second column), and the probability of the occurrence of extreme precipitation (third column).

4.2 Assessment of U-Net variants

Motivated by the good performance of U-Net in simulating precipitation events, we conducted further experiments to assess the predictive capabilities of several U-Net-based architectures only for precipitation events.

4.2.1 U-Net with attention

Recently, within the attention framework, Trebing et al. (2021) proposed an adapted U-Net with a combination of attention modules and depthwise-separable convolutions for precipitation nowcasting. Introducing an attention mechanism into the convolutional neural network structure has also become popular in image segmentation processes (Oktay et al., 2018). In particular, the Attention U-Net proposed by Oktay et al. (2018) exploits the use of Attention Gates added to the encoder-decoder structure. This soft-attention mechanism is implemented for the skip connections. The Attention Gates actively suppresses activations in irrelevant regions and, thus, reduces the number of redundant features. The authors showed that the use of Attention Gates improved the prediction performance of U-Net as the model learned to focus on useful features information, enhancing the accuracy of the network in locating tissues and organs, in the medical context. Based on this, we also tested whether the inclusion of Attention Gates improve the accuracy of simulating extreme precipitation events. While using an attention gate in U-Net showed an improvement for medical image datasets (Oktay et al., 2018), this was not the case in our application, as the results showed similar performances with or without the attention gates (Table 6). Therefore, the attention gates were not further used in the following analyses.

Table 6. Scores of the original U-Net and the U-Net with attention when trained to predict heavy precipitation. Precision and recall are computed for the exceedance of the 95th percentile.

Model id	AUC train	AUC test	Precision train	Precision test	Recall train	Recall test
U-Net	0.987	0.980	0.384	0.387	0.979	0.950
U-Net Attention	0.986	0.981	0.378	0.382	0.983	0.953

4.2.2 Sensitivity to U-Net depth and number of features

As the U-Net hyperparameters, such as the network depth or the number of feature maps, greatly affect the number of trainable weights and the model performance, we explored the effect of the U-Net architecture design on the prediction of precipitation events, in particular, heavy precipitation events. Thus, we conducted several sensitivity analyses to explore whether reducing the number of hyperparameters would lead to comparable results to the original U-Net. Specifically, we focused on the architecture size, i.e., the depth of the network that we measured in terms of the number of *encoder-decoder* levels. Starting from the original network made of 4 levels (Ronneberger et al., 2015), we decreased the number of levels (i.e., network depth) iteratively until the simplest network (i.e., 1 level).

In addition, for each U-Net-based network, we further assessed the importance of the predictors in the model performance. With the feature selection, we aim to assess whether reducing the number of features, which would also reduce the computational effort, results in a similar or better performance than the full set of features (i.e., 31). A typical forward/backward stepwise selection procedure where the predictors are included/removed one at a time would be computationally expensive. Thus, the predictors were included in

383 the models five at a time according to the ranking provided by the LRP (see Fig. 3). For
 384 example, the first subset consists of the top five predictors (RH700, V1000, RH850, RH500,
 385 and U1000), the second subset includes the top ten predictors, and so on.

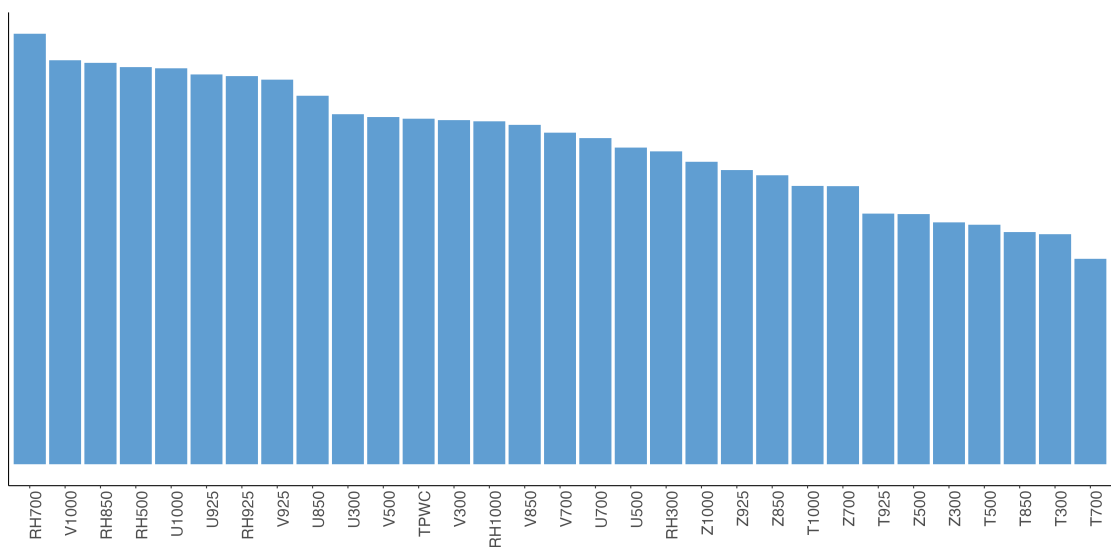


Figure 3. Ranked relevances (averages) obtained for heavy precipitation events in the training sample (1979-2005) for each feature.

386 By jointly varying the architecture depth and the number of inputs, we assessed four
 387 U-Net architectures, each one trained separately for 6 predictor subsets, resulting in a total
 388 of 30 models (four levels and six predictor subsets). It is important to note that all models
 389 were trained separately. As the size of the architecture is reduced, the number of trainable
 390 parameters considerably decreases (Fig. 4).

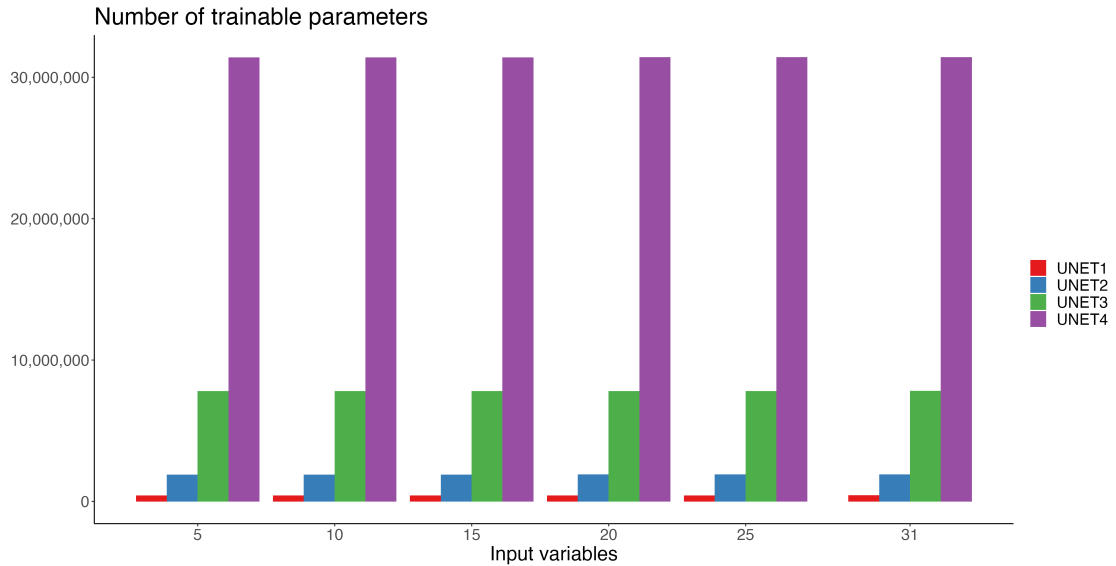


Figure 4. Number of trainable parameters for the different architecture sizes for the different subsets of predictors. Note that the number of trainable parameters changes with the number of input data even though the changes are small.

391 As stated in the previous Section, we evaluate the forecast skill of heavy precipitation
 392 events through the categorical skill scores commonly used for classification problems and
 393 can be obtained from the contingency table. The AUC, precision, and recall scores were
 394 calculated for both training and test datasets. Figure 5 illustrates the results corresponding
 395 to the U-Net architectures used in the experiments for different subsets of predictors.

396 It can be observed that the performance is considerably lower for the input of 5 features
 397 and improves when increasing the number of predictors to 10 or 15. Overall, the proportion
 398 of heavy precipitation events that are correctly classified (i.e., precision) is higher when
 399 increasing the number of features for the deeper U-Nets (e.g., UNET3, UNET4). However,
 400 such skill improvement with the number of features is not observed for the shallowest U-
 401 Nets (UNET1, UNET2) and the models show the highest precision when using 15 and 20
 402 features. It should be noted that these optimums likely depend on the random seed and
 403 some variability is expected between different random seeds. These results show anyway
 404 that more data does not always means better performance. The recall values tend to increase
 405 with the number of predictors, but only up to 10 or 15 features.

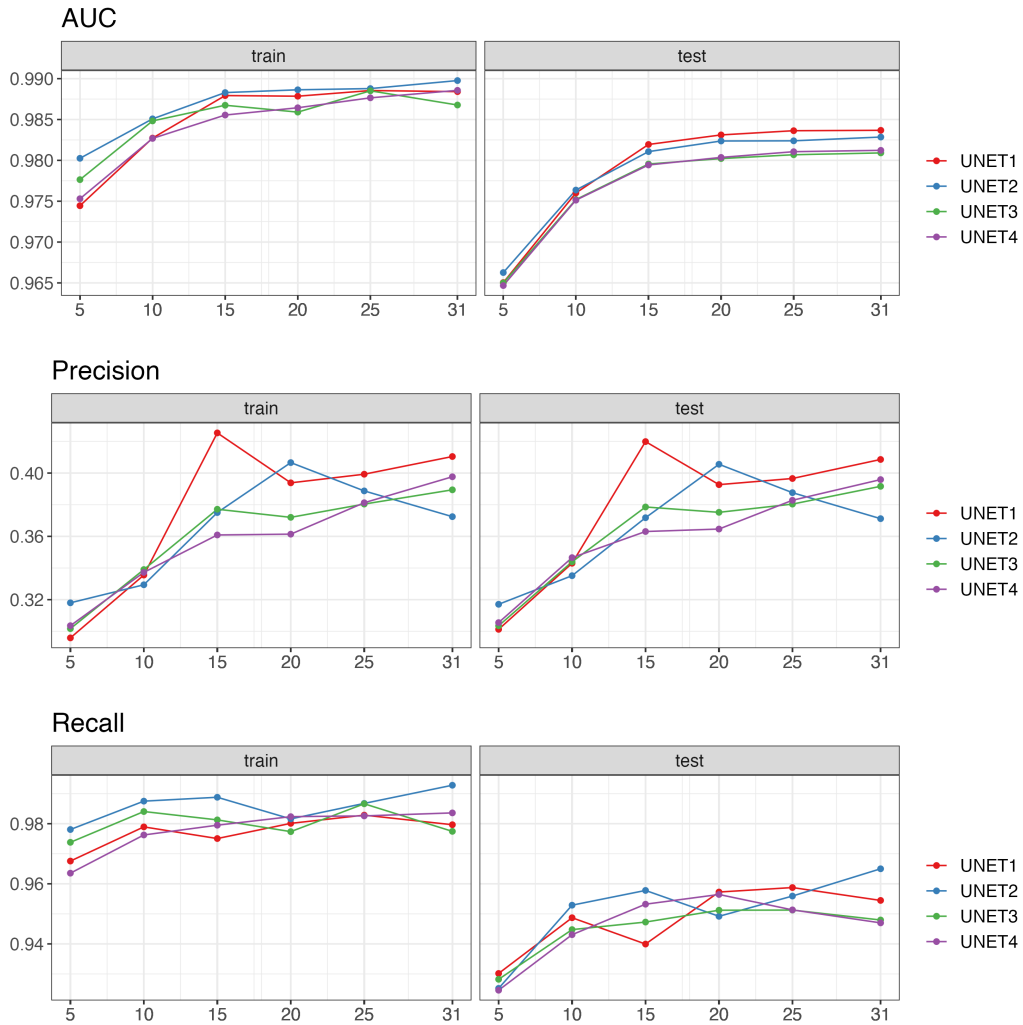


Figure 5. Scores obtained for the U-Net-based networks: U-Net1 (1 levels), U-Net2 (2 levels), U-Net3 (3 levels) and U-Net4 (4 levels) for different subsets of predictors according to the LRP-ranking.

406

4.3 Interpretability: LRP

407

408

409

410

411

412

413

414

415

416

417

418

419

The LRP previously used was also mapped to visualize which features and which geographical region are important for the U-Net network to predict a heavy precipitation event. We first examined the composite LRP maps (Sect. 3.2.3) for all heavy events occurring during the training period (1979-2005). These maps highlight the relevant features at a pixel scale for predicting heavy precipitation at that same pixel (Fig. 6). Note that we apply the α - β rule, which only considers positive activations. From Figure 6 it can be observed that some features are more relevant inland (e.g., relative humidity fields) while others have an increased relevance for events occurring over the sea (e.g., geopotential height). Overall, the relative humidity shows the highest values, followed by both wind components, particularly in western and southern Europe. The high relevance of the wind components in some areas reflects the dependence between extreme precipitation events and strong wind conditions due to the same mesoscale and/or synoptic features, as shown by previous studies (Martius et al., 2016). For example, one can observe the higher relevance values of the zonal

420 (e.g., U850, U925) and meridional wind (e.g., V925) in the Iberian Peninsula, which often
 421 experiences concurrent extreme precipitation and winds conditions, mostly related to extra-
 422 tropical cyclones and their atmospheric fronts (Hénin et al., 2021). We can also distinguish
 423 the relevance of the meridional wind (e.g., V500) for the alpine region, which is known to
 424 be related to heavy precipitation events due to the orographic forcing of air masses that
 425 transport moisture from the Mediterranean. This influence of the atmospheric circulation
 426 comes in pair with the moisture information, heavily represented by the relative humidity
 427 variable at 700 hPa (RH700).

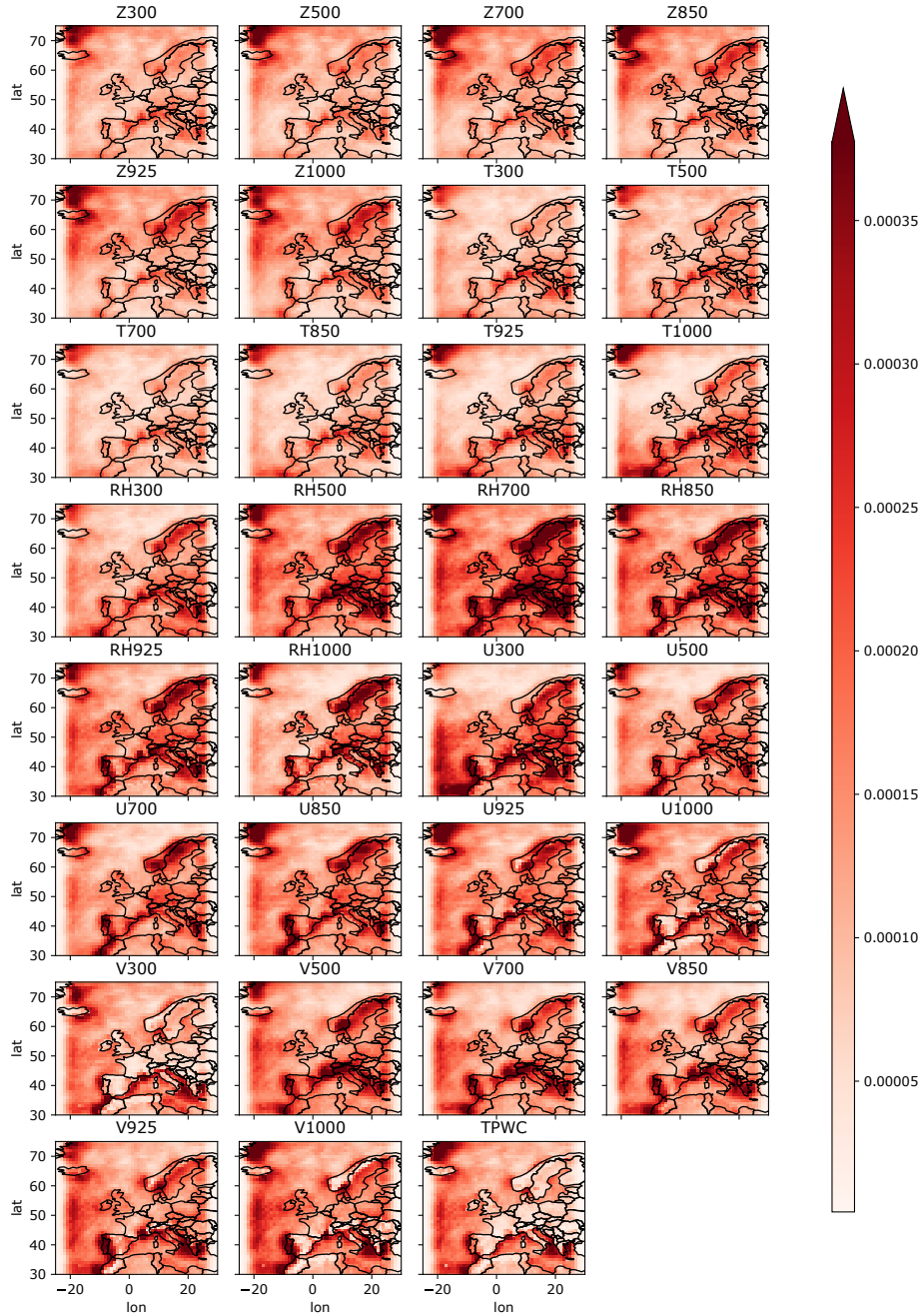


Figure 6. Composite relevance maps for heavy precipitation events ($> 95th$ percentile) derived from the U-Net original architecture during the training period (1979-2005) for each feature.

428 We then examined the relevance of predictors for single extreme precipitation events,
 429 starting by analyzing the same event that led to the highest amount of observed precipitation
 430 exceeding the 95th percentile (Figure 1). The meteorological context during that day, 13th
 431 October 2018, was characterized by an extra-tropical cyclone called Leslie, which was a large
 432 long-lived tropical cyclone in the Atlantic that became a powerful post-tropical system and
 433 made land in Portugal on 13th October (Mandement & Caumont, 2021). This remarkable
 434 event resulted in heavy precipitation in several regions in Western Europe (e.g., Portugal,
 435 France). Also that day, another storm called Callum that began as an Atlantic depression
 436 led to strong winds and flooding over the U.K.

437 After calculating the LRP for the days during that particular episode (13-15 October
 438 2018) for each feature, we averaged them over all input variables. Figure 7 illustrates the
 439 temporal evolution of the influence of the inputs for the precipitation event. The maps show
 440 the regions that are physically related to precipitation extremes. For example, on the 13th
 441 October the networks focus on the U.K., as the region of influence, although late the same
 442 day, another storm reached the western coast of Portugal. It must be noted that we use
 443 daily averages, therefore, it seems reasonable for the model to look at the regions where
 444 the inputs have major weights. It can be observed how the region of influence shifts south-
 445 eastwards, which is physically consistent with the development of the synoptic situation
 446 associated with that heavy precipitation episode (Mandement & Caumont, 2021).

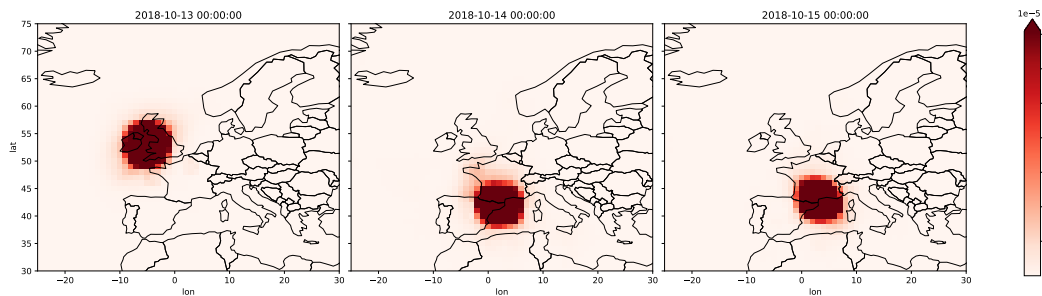


Figure 7. Temporal evolution of the averaged relevance over all input variables during the episode of October 2018.

447 In addition, we analyzed another episode of heavy precipitation that occurred in sum-
 448 mer 2021, specifically during the period 13th to 15th July 2021, which led to severe flooding,
 449 particularly in North Rhineland-Palatinate in Germany, part of Belgium, and the Nether-
 450 lands (Kreienkamp, 2022). While the U-Net is able to capture this episode, a larger spatial
 451 extension was predicted, indicating that the model overestimates the geographical area af-
 452 fected by the event (e.g., see Figure S3). This is expected due to a higher number of *False*
 453 *positive*, as shown by the precision skill score (see Table 3).

454 Similar to the episode of October 2018, the model tends to look at the geographical
 455 region where heavy rainfall occurred (e.g., western and central Europe, see Figure S4). The
 456 LRP maps for this event show similar patterns for all the input features with a common area
 457 of higher relevance in the Netherlands, Belgium, northwest of France, and west of Germany.
 458 As shown in Fig. 7, the network finds the most relevant geographical regions at the same
 459 location as the heavy precipitation event evolves. This indicates that the local predictors

460 contain enough information to predict the event and that no remote information is needed.
461 The LRP maps focus on the regions physically related to the episode, and no relevant areas
462 are found outside central and west of Europe.

463 5 Conclusions

464 The use of machine learning has exponentially grown in the past years in a wide number
465 of fields. In particular, deep learning methods have shown enormous potential to address
466 complex Earth Science problems, which might be useful to tackle climate change-related
467 issues. Here, we have presented an intercomparison of existing architectures used to predict
468 precipitation, either for aggregated precipitation (i.e., over an extended region) or spatial
469 precipitation fields. A total of six models consisting of different CNN configurations were
470 tested. We examined the forecast skill not only to simulate heavy and extreme precipitation
471 events but also to predict the amount of precipitation over the European domain. For the
472 interpretability of the networks, we applied a layer-wise propagation technique, which was
473 further used as a tool of feature selection to test the importance of the number of input
474 parameters on the model performance. It is important to note that while some of these
475 DL topologies have been previously presented in the literature, the original application
476 slightly differs from ours, and more importantly, the original configuration was adapted to
477 our purposes (e.g., in each case, we added a decoder part to preserve the spatial dimensions
478 of the input data).

479 In general, most of the analyzed DL were able to reproduce reasonably well the occur-
480 rence of precipitation events. However, we found that the U-Net outperformed the rest of
481 the tested architectures by a large margin, which is in line with previous studies (Hess &
482 Boers, 2022; Larraondo et al., 2019) that used a U-Net architecture to simulate precipita-
483 tion. In general, the skill scores that measure the precision to classify heavy precipitation
484 events (i.e., >95th percentile) were higher than those obtained for extreme precipitation
485 events (i.e., >99th percentile), due to the unbalanced number of classes where the number
486 of extremes is significantly reduced in the training data.

487 Motivated by the good performance shown by the U-Net architecture, we additionally
488 conducted a number of experiments on U-Net-based configurations to examine how the
489 network depth and the number of inputs play a role in the performance of the model. As
490 expected, the network showed the poorest performance when using only a few input variables
491 for all the U-Net-based networks (i.e., different levels of depth). Overall, a deeper network
492 achieves slightly better results with the largest number of inputs, especially regarding the
493 precision scores. On the contrary, shallower networks seem to achieve similar skill scores
494 for a lower number of input data. We noticed that from 15 features on, the models only
495 gained a modest improvement overall, suggesting that a smaller number of input would lead
496 to similar results with less computational effort.

497 While the original U-Net already showed a good performance, we found that a shallower
498 network, in terms of number levels compared to the original architecture, would be sufficient
499 to classify heavy precipitation events correctly. This likely means that, for this spatial
500 resolution and with no temporal extrapolation, most of the information needed to forecast
501 precipitation is available at the location where the precipitation occurs. Our results showed
502 that in such a context, a shallower U-Net, which significantly reduces the number of trainable
503 parameters and the computationally time, is able to predict fairly well precipitation events.

504 6 Data Availability Statement

505 The ERA5 data is available for download at the Copernicus Climate Change Service
506 (C3S; Hersbach et al., 2020; <https://cds.climate.copernicus.eu/cdsapp#!/dataset/reanalysis-era5-pressure-levels>). The code used for the analysis is available in:
507 <https://github.com/ML-precip/precip-predict>
508

References

- 509
- 510 Adewoyin, R. A., Dueben, P., Watson, P., He, Y., & Dutta, R. (2021). TRU-NET: a deep
511 learning approach to high resolution prediction of rainfall. *Machine Learning*, *110*(8),
512 2035–2062. doi: 10.1007/s10994-021-06022-6
- 513 Ayzel, G., Heistermann, M., Sorokin, A., Nikitin, O., & Lukyanova, O. (2019). All convo-
514 lutional neural networks for radar-based precipitation nowcasting. *Procedia Computer
515 Science*, *150*, 186–192. doi: 10.1016/j.procs.2019.02.036
- 516 Barnes, E. A., Barnes, R. J., Martin, Z. K., & Rader, J. K. (2022). This looks like that
517 there: Interpretable neural networks for image tasks when location matters. *Earth
518 and Space Science Open Archive*, *34*. doi: 10.1002/essoar.10509984.2
- 519 Bauer, P., Thorpe, A., & Bruner, G. (2015). The quiet revolution of numerical weather
520 prediction. *Nature*, *525*, 47–55. doi: 10.1038/nature14956
- 521 Chattopadhyay, A., Hassanzadeh, P., & Pasha, S. (2020). Predicting clustered weather
522 patterns: A test case for applications of convolutional neural networks to spatio-
523 temporal climate data. *Sci Rep*, *10*, 1317. doi: 10.1038/s41598-020-57897-9
- 524 Chollet, F. (2017). Xception: Deep learning with depthwise separable convolutions. In *2017
525 ieee conference on computer vision and pattern recognition (cvpr)* (p. 1800–1807). doi:
526 10.1109/CVPR.2017.195
- 527 Chollet, F., et al. (2015). *Keras*. <https://github.com/fchollet/keras>. GitHub.
- 528 Civitarese, D. S., Szwarcman, D., Zadrozny, B., & Watson, C. (2021). Extreme Precipita-
529 tion Seasonal Forecast Using a Transformer Neural Network. *arXiv*. Retrieved from
530 <http://arxiv.org/abs/2107.06846>
- 531 Davenport, F. V., & Duffenbaugh, N. S. (2021). Using Machine Learning to Analyze Physical
532 Causes of Climate Change: A Case Study of U.S. Midwest Extreme Precipitation.
533 *Geophysical Research Letters*, *48*(15). doi: 10.1029/2021GL093787
- 534 Donat, M., Lowry, A., Alexander, L., P., O., Maher, N., & Duffenbaugh, N. S. (2016). More
535 extreme precipitation in the world’s dry and wet regions. *Nature Clim Change*, *6*,
536 508–513. doi: 10.1038/nclimate2941
- 537 Gao, X., & A., S. C. (2019). Mid-Western US heavy summer-precipitation in regional and
538 global climate models: the impact on model skill and consensus through an analogue
539 lens. *Clim Dyn*, *6*, 1569–1582. doi: 10.1007/s00382-018-4209-0
- 540 Gelaro, R., McCarty, W., Suárez, M. J., Todling, R., Molod, A., Takacs, L., . . . Zhao, B.
541 (2017). The modern-era retrospective analysis for research and applications, version
542 2 (MERRA-2). *J. Climate*, *30*(14), 5419–5454. doi: 10.1175/JCLI-D-16-0758.1
- 543 Goodfellow, I., Bengio, Y., & Courville, A. (2016). *Deep learning*. MIT Press. Retrieved
544 from <http://www.deeplearningbook.org>
- 545 Grönquist, P., Yao, C., Ben-Nun, T., Dryden, N., Dueben, P., Li, S., & Hoefler, T. (2021).
546 Deep learning for post-processing ensemble weather forecasts. *Philosophical Trans-
547 actions of the Royal Society A: Mathematical, Physical and Engineering Sciences*,
548 *379*(2194), 20200092. doi: 10.1098/rsta.2020.0092
- 549 Hersbach, H., Bell, B., Berrisford, P., Hirahara, S., Horányi, A., Muñoz-Sabater, J., . . .
550 Thépaut, J. N. (2020). The ERA5 global reanalysis. *Quarterly Journal of the Royal
551 Meteorological Society*, *146*(730), 1999–2049. doi: 10.1002/qj.3803
- 552 Hess, P., & Boers, N. (2022). Deep learning for improving numerical weather pre-
553 diction of heavy rainfall. *Journal of Advances in Modeling Earth Systems*, *14*(3),
554 e2021MS002765. doi: 10.1029/2021MS002765
- 555 Horton, P. (2021). Analogue methods and ERA5 : Benefits and pitfalls. *International
556 Journal of Climatology*(November), 1–19. doi: 10.1002/joc.7484
- 557 Huang, W. (2022). Extreme precipitation forecasting using attention augmented con-
558 volutions. *CoRR*, *abs/2201.13408*. Retrieved from [https://arxiv.org/abs/2201](https://arxiv.org/abs/2201.13408)
559 [.13408](https://arxiv.org/abs/2201.13408)
- 560 Hwang, J., Orenstein, P., Cohen, J., Pfeiffer, K., & Mackey, L. (2019). Improving sub-
561 seasonal forecasting in the western U.S. With machine learning. *Proceedings of the
562 ACM SIGKDD International Conference on Knowledge Discovery and Data Mining*,
563 2325–2335. doi: 10.1145/3292500.3330674

- 564 Hénin, R., Ramos, A. M., Pinto, J. G., & Liberato, M. L. R. (2021). A ranking of concurrent
565 precipitation and wind events for the Iberian peninsula. *International Journal of*
566 *Climatology*, *41*(2), 1421-1437. doi: 10.1002/joc.6829
- 567 Kreienkamp, e. a., F. (2022). Rapid attribution of heavy rainfall events leading to
568 the severe flooding in Western Europe during July 2021. *World Weather Attri-*
569 *bution*. Retrieved from [https://www.worldweatherattribution.org/wp-content/](https://www.worldweatherattribution.org/wp-content/uploads/Scientific-report-Western-Europe-floods-2021-attribution.pdf)
570 [uploads/Scientific-report-Western-Europe-floods-2021-attribution.pdf](https://www.worldweatherattribution.org/wp-content/uploads/Scientific-report-Western-Europe-floods-2021-attribution.pdf)
- 571 Larraondo, P. R., Renzullo, L. J., Inza, I., & Lozano, J. A. (2019). A data-driven approach to
572 precipitation parameterizations using convolutional encoder-decoder neural networks.
573 *arXiv*. doi: 10.48550/ARXIV.1903.10274
- 574 LeCun, Y., & Bengio, Y. (1995). Convolutional networks for images, speech, and time
575 series, the handbook of brain theory and neural networks. *MIT Press*, 255–258.
- 576 Liu, Y., Racah, E., Prabhat, Correa, J., Khosrowshahi, A., Lavers, D., ... Collins, W.
577 (2016). Application of deep convolutional neural networks for detecting extreme
578 weather in climate datasets. *arXiv*.
- 579 Mandement, M., & Caumont, O. (2021). A numerical study to investigate the roles of
580 former hurricane Leslie, orography and evaporative cooling in the 2018 Aude heavy-
581 precipitation event. *Weather Clim. Dynam.*, *2*, 795–818. doi: 10.5194/wcd-2-795
582 -2021
- 583 Maraun, D., M., W., & J.M., G. (2017). Statistical downscaling skill under present climate
584 conditions: A synthesis of the value perfect predictor experiment. *Int J Climatol.*, *39*,
585 3692-3703. doi: 10.1002/joc.5877
- 586 Martius, O., Pfahl, S., & Chevalier, C. (2016). A global quantification of compound pre-
587 cipitation and wind extremes. *Geophysical Research Letters*, *43*(14), 7709-7717. doi:
588 10.1002/2016GL070017
- 589 Montavon, G., Samek, W., & Müller, K.-R. (2018). Methods for interpreting and
590 understanding deep neural networks. *Digital Signal Processing*, *73*, 1-15. doi:
591 10.1016/j.dsp.2017.10.011
- 592 Oktay, O., Schlemper, J., Folgoc, L. L., Lee, M., Heinrich, M., Misawa, K., ... Rueckert,
593 D. (2018). *Attention u-net: Learning where to look for the pancreas*. arXiv. doi:
594 10.48550/ARXIV.1804.03999
- 595 Pan, B., Hsu, K., AghaKouchak, A., & Sorooshian, S. (2019). Improving precipitation
596 estimation using convolutional neural network. *Water Resources Research*, *55*(3),
597 2301-2321. doi: 10.1029/2018WR024090
- 598 Racah, E., Beckham, C., Maharaj, T., Prabhat, & Pal, C. J. (2016). Semi-supervised
599 detection of extreme weather events in large climate datasets. *CoRR*, *abs/1612.02095*.
600 Retrieved from <http://arxiv.org/abs/1612.02095>
- 601 Rasp, S., Dueben, P. D., Scher, S., Weyn, J. A., Mouatadid, S., & Thuerey, N. (2020, Nov).
602 Weatherbench: A benchmark data set for data-driven weather forecasting. *Journal of*
603 *Advances in Modeling Earth Systems*, *12*(11). doi: 10.1029/2020ms002203
- 604 Ronneberger, O., Fischer, P., & Brox, T. (2015). U-Net: Convolutional Networks for
605 Biomedical Image Segmentation. In N. Navab et al. (Eds.), *Medical image computing*
606 *and computer-assisted intervention – miccai 2015* (pp. 234–241). Springer Interna-
607 tional Publishing. doi: 10.1007/978-3-319-24574-4_28
- 608 Scher, S. (2018). Toward data-driven weather and climate forecasting: Approximating a
609 simple general circulation model with deep learning. *Geophysical Research Letters*,
610 *45*(22), 12,616-12,622. doi: 10.1029/2018GL080704
- 611 Schultz, M. G., Betancourt, C., Gong, B., Kleinert, F., Langguth, M., Leufen, L. H., ...
612 Stadtler, S. (2021). Can deep learning beat numerical weather prediction? *Philo-*
613 *sophical Transactions of the Royal Society A: Mathematical, Physical and Engineering*
614 *Sciences*, *379*(2194). doi: 10.1098/rsta.2020.0097
- 615 Shi, X. (2020). Enabling smart dynamical downscaling of extreme precipitation events
616 with machine learning. *Geophysical Research Letters*, *47*(19), e2020GL090309. doi:
617 10.1029/2020GL090309
- 618 Shi, X., Chen, Z., Wang, H., Yeung, D., Wong, W., & Woo, W. (2015). Convolutional

- 619 LSTM network: A machine learning approach for precipitation nowcasting. *CoRR*,
620 *abs/1506.04214*. Retrieved from <http://arxiv.org/abs/1506.04214>
- 621 Shi, X., Gao, Z., Lausen, L., Wang, H., Yeung, D., Wong, W., & Woo, W. (2017).
622 Deep learning for precipitation nowcasting: A benchmark and A new model. *CoRR*,
623 *abs/1706.03458*. Retrieved from <http://arxiv.org/abs/1706.03458>
- 624 Toms, B. A., Barnes, E. A., & Imme, E.-U. (2020). Physically interpretable neural networks
625 for the geosciences: Applications to earth system variability. *Journal of Advances in*
626 *Modeling Earth Systems*, *12*(9), e2019MS002002. doi: 10.1029/2019MS002002
- 627 Trebing, K., Stańczyk, T., & Mehrkanoon, S. (2021). Smaat-unet: Precipitation nowcasting
628 using a small attention-unet architecture. *Pattern Recognition Letters*, *145*, 178-186.
629 doi: 10.1016/j.patrec.2021.01.036
- 630 Trenberth, K., Dai, A., Rasmussen, R. M., & Parsons, D. B. (2003). The changing character
631 of precipitation. *Bull. Am. Meteorol. Soc.*(84), 1205-1218. doi: 10.1175/BAMS-84-9
632 -1205
- 633 Vandal, T., Kodra, E., & Ganguly, A. R. (2019). Intercomparison of machine learning meth-
634 ods for statistical downscaling: the case of daily and extreme precipitation. *Theoretical*
635 *and Applied Climatology*, *137*(1-2), 557–570. doi: 10.1007/s00704-018-2613-3
- 636 Weyn, J. A., Durran, D. R., & Caruana, R. (2019). Can machines learn to predict weather?
637 using deep learning to predict gridded 500-hpa geopotential height from historical
638 weather data. *Journal of Advances in Modeling Earth Systems*, *11*(8), 2680-2693. doi:
639 10.1029/2019MS001705
- 640 Weyn, J. A., Durran, D. R., & Caruana, R. (2020). Improving data-driven global weather
641 prediction using deep convolutional neural networks on a cubed sphere. *Journal*
642 *of Advances in Modeling Earth Systems*, *12*(9), e2020MS002109. doi: 10.1029/
643 2020MS002109

1 **Supporting Information for Intercomparison of deep**
 2 **learning architectures for the prediction of**
 3 **precipitation fields**

4 **Noelia Otero and Pascal Horton**

5 ¹Institute of Geography and Oeschger Centre for Climate Change Research, University of Bern, Bern,
 6 Switzerland

7 This supporting information contains the following figures:

- 8 • Figure S1 shows the spatial distribution of precipitation events.
- 9 • Figure S2 shows the evolution during the training for modelling precipitation amounts.
- 10 • Figure S3 shows the evolution during the training for modelling extreme precip-
- 11 itation.
- 12 • Figure S4 shows the observed and predicted precipitation extremes (>95th per-
- 13 centile).
- 14 • Figure S5 shows the temporal evolution of the relevance averaged over all input
- 15 variables during a heavy rainfall event in summer 2021.

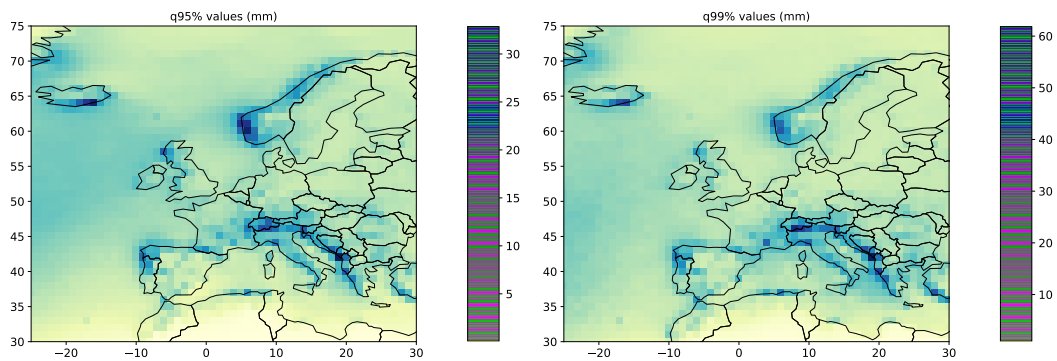


Figure 1. Spatial distribution of the 95th and 99th percentiles of the precipitation corresponding to the whole period of study (1979-2021).

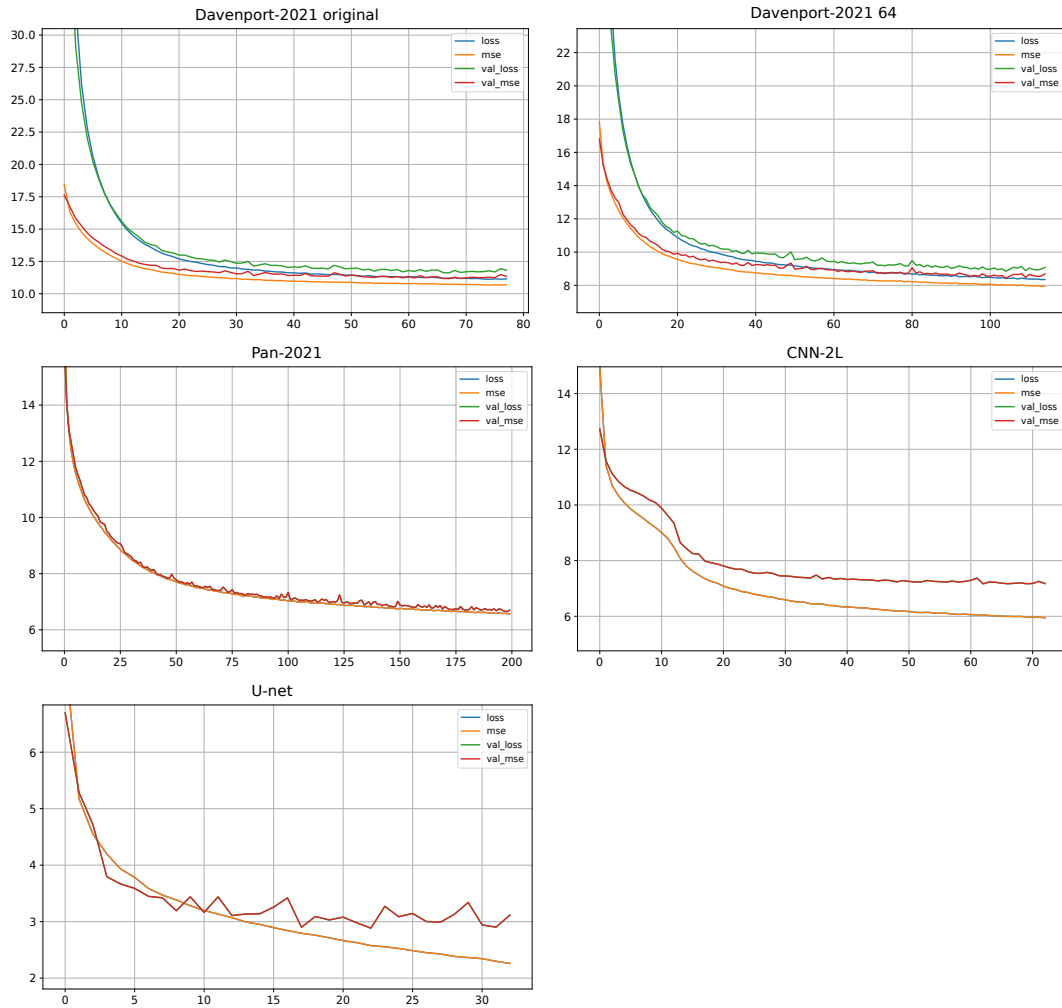


Figure 2. Training and validation loss for the selected models when simulating the amount of precipitation..

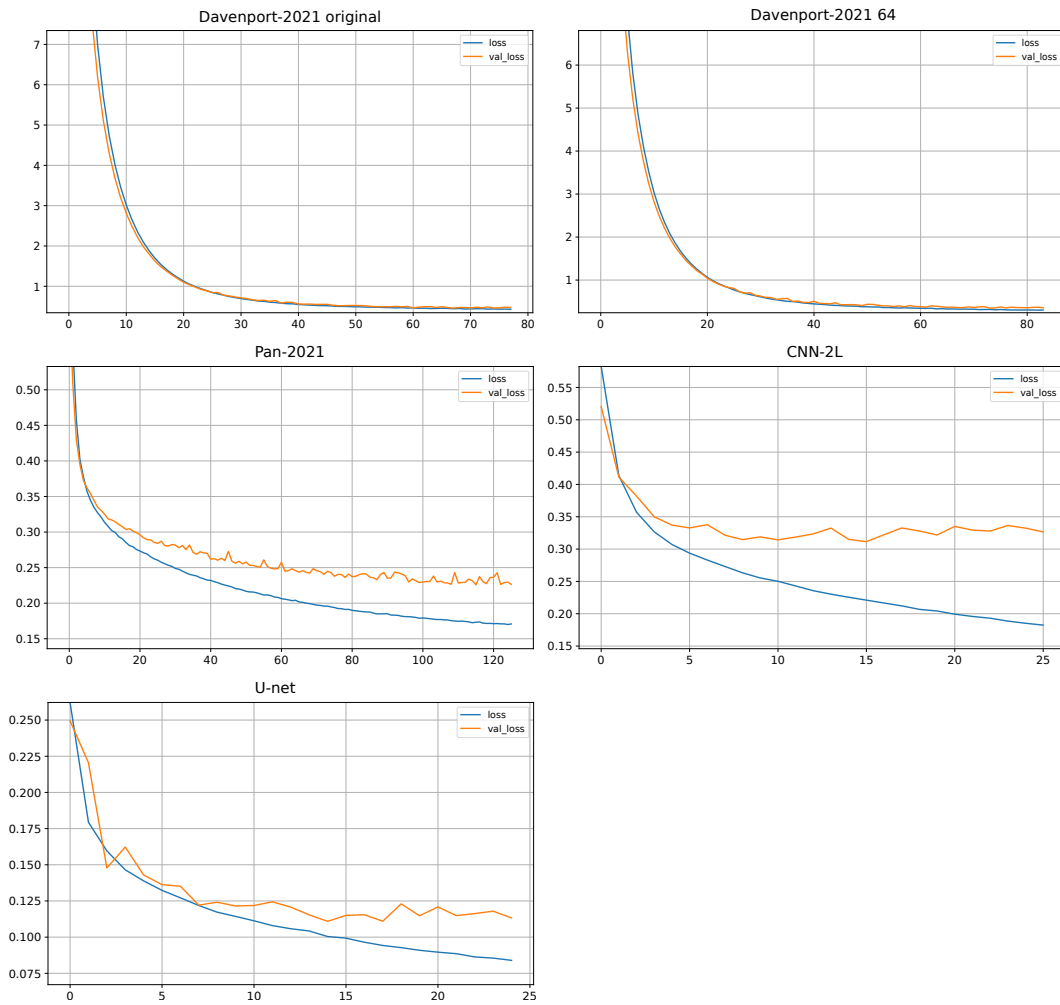


Figure 3. raining and validation loss for the selected models when simulating precipitation extremes (>99th percentile).

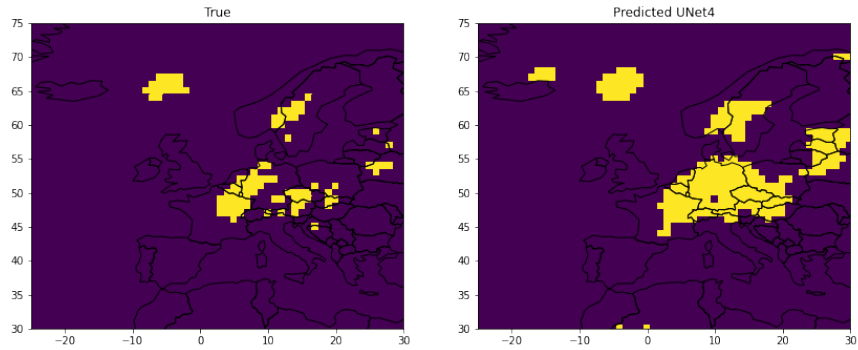


Figure 4. Observed precipitation exceedances (>95th percentile) occurred during the heavy rainfall event of summer 2021, on the 14 July 2021 (left) and U-Net predicted exceedances for the same day (right).

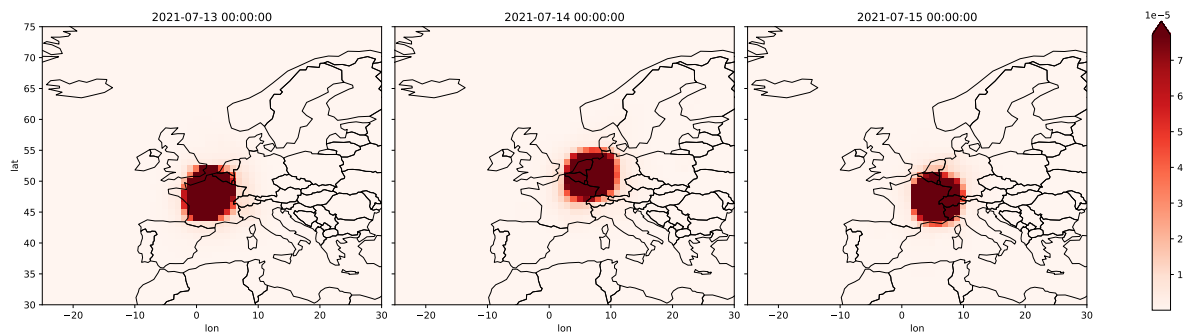


Figure 5. Temporal evolution of the mean of relevance over all input variables during the episode of October 2021.